AIAA 2002–3066

Modeling of the Wake Behind a Circular Cylinder Undergoing Rotational Oscillation

Douglas R. Smith
Department of Mechanical Engineering
University of Wyoming
P.O. Box 3295
Laramie, WY 82071-3295

Stefan Siegel Thomas McLaughlin
Department of Aeronautics
US Air Force Academy
US Air Force Academy, CO 80840

1st AIAA Flow Control Conference
24–26 June 2002 / St. Louis, MO

AIAA 2002–3066

Modeling of the Wake Behind a Circular Cylinder Undergoing Rotational Oscillation

Douglas R. Smith*
Department of Mechanical Engineering
University of Wyoming
P.O. Box 3295
Laramie, WY 82071-3295

Stefan Siegel†
Thomas McLaughlin‡
Department of Aeronautics
US Air Force Academy
US Air Force Academy, CO 80840

A short experimental program was undertaken to evaluate the effect of low-amplitude rotational oscillations on the wake of a circular cylinder at low Reynolds number (Re = 125). Using the experimental data, a low-dimensional model of the wake was developed and evaluated. The experimental results reveal that the wake undergoes a transition from the Karman vortex street to an asymmetric, with respect to the wake centerline, shedding pattern at a critical value of the forcing ($\Omega_1 \approx 1$). A POD analysis of the experimental measurements reveal that the transition is quite abrupt, and that the new wake state is of approximately the same dimension as the Karman vortex street. The low-dimensional model of the flow qualitatively captures the vortex dynamics in the wake with relatively few modes.

Introduction

THE wake of a circular cylinder at low Reynolds number is the archetype for a flow exhibiting self-sustained oscillations as a result of a hydrodynamic resonance. At a Reynolds number above 50, this wake oscillation is manifested as the Karman vortex street. Abernathy and Kronauer[1] linked the formation of the vortex street to an instability in the wake. Later Koch[2] identified that a direct resonance condition is present in symmetric blunt body wakes. He connected this condition to a region of absolute instability in the near wake and the appearance of a vortex street. Triantafyllou et al.[3] used a linear stability analysis to show that an absolute instability in a symmetric wake mode permits disturbances to grow temporally at a fixed spatial location in the near-wake. The non-linearities in the flow limit the disturbance amplitude and ultimately a self-sustained oscillation is established. The absolute instability, however, is only a necessary condition for the formation of the vortex street. Chomaz et al.[4] revealed that the length of the recirculation region must reach a critical length before the resonances that lead to the vortex sheet occur. The work of Provansal et al.,[5] Monkewitz[6] and others further established the steady-periodic Karman vortex sheet as the result of a saturated temporal global wake instability. From the perspective of control, the circular cylinder wake behaves as a non-linear, self-excited oscillator that responds in a manner similar to a van der Pol oscillator when subject to external forcing.[5]

For reasons related to flow-induced vibrations, it is frequently of interest to *suppress* the oscillation in the cylinder wake. This effect can be achieved if the instability can be controlled but requires feedback because of the non-linear nature of the oscillation. It also requires a control input to the wake through, for example, some motion of the cylinder. Below, we consider briefly the wake response to forcing from the cylinder.

Wake Response to Forcing

The Karman vortex street induces an unsteady transverse force at the cylinder, and under certain conditions, when the cylinder is free to move, these forces can lead to a resonance condition with large amplitude cylinder oscillations. Where circular cylinders appear in industrial applications, the oscillations can lead to structural damage and structure failure.

*Assistant Professor, Senior Member AIAA
†NRC Postdoctoral Fellow, Member AIAA
‡Senior Member AIAA

From a phenomenological perspective, the flow-induced vibration is hydrodynamically the same as a forced cylinder oscillation, and it is possible to understand the wake dynamics by exploring the response of the wake to excitations imposed by the cylinder. There are many ways in which to introduce forcing to the cylinder wake, and perhaps because the wake is a relatively low-dimensional system, the responses are quite similar regardless of the inputs.[7] Transverse translational motion of the cylinder is perhaps the most common method of forcing, but acoustic,[7,8] in-line motion[9] and rotational forcing[10–12] have also been studied.

We can summarize some of the more general features of the wake in response to forcing (see also Griffin and Hall[13]). To start we note that at low Reynolds numbers (Re = 100–200) the wake response does not appear to depend on Reynolds number.[7] Typically, the wake of a circular cylinder contains vortices shed with an oblique orientation relative to the cylinder axis. The introduction of forcing increases the spanwise coherence of the shedding and parallel vortices ensue. Not unexpectedly, the wake is most receptive to forcing at its natural shedding frequency or harmonics thereof, and forcing at quite low levels produces lock-on where the shedding assumes the frequency of the forcing. A plot of the forcing amplitude versus the forcing frequency shows a V-shaped lock-on regime with the apex at the natural shedding frequency (see figure 3.10, Blevins[14]). This behavior is characteristic of a van der Pol oscillator. The state assumed by the wake will depend on the forcing frequency and amplitude. Using acoustic excitation in the mean flow direction (creating an effect similar to in-line oscillation), Detemple-Laake and Eckelmann[7] found twelve wake structures appearing in three frequency regimes. The widest variety of structures were found for a forcing frequency at one-half the natural shedding frequency. Here, seven different structures were observed including "sea-horse" shapes, vortex twins (vortex pairs arranged symmetrically about the wake centerline) and vortex triplets (where two vortices are shed from one side of the cylinder). From a modeling perspective, these different wake structures represent different (higher order) modes that must be adequately represented in any model of the wake. Three-dimensional effects are also present in the wake even when the spanwise coherence is high, and their impact on the wake cannot be neglected in any model.[15]

The work to be described in this paper focusses on one aspect, flow modeling, in the development of a closed-loop control scheme for the cylinder wake. Feedback control of the cylinder wake was first accomplished by Berger[16] in 1967, and in recent years has received renewed attention with varying degrees of success. To provide perspective on the work to be discussed later, we review some of this recent work.

Wake Control

In the last decade, there have been quite a few investigations using closed-loop, or feedback, control on the low Reynolds number cylinder wake. Using feedback control with acoustic forcing, Roussopoulos[17] was able to suppress the wake instability at Reynolds numbers just above the onset of vortex shedding (Re=48). A single sensor was used in the experiments, and the instability was only suppressed in the vicinity of the sensor. Away from the sensor location however, the wake was largely unaffected by the control.

Park et al.[18] computationally studied feedback control of the wake stability at Reynolds numbers of 60 and 80. A single sensor was used for feedback, and the control input was blowing and suction through slots located on the aft portion of the cylinder. They demonstrated complete suppression of vortex shedding at Re = 60, but at the higher Reynolds number, the feedback control tended to excite a secondary mode at a frequency lower than the natural shedding frequency. They also observed that feedback control occurs for an optimal location for the sensor in the wake.

Expanding on the earlier work of Roussopoulos,[17] Roussopoulos and Monkewitz[15] used a two-dimensional Ginzburg-Landau equation to study feedback control at Re = 47 with the three-dimensional effects from along the span of the cylinder. A single sensor was used for feedback. Their results confirm that with a single sensor steady state suppression of vortex shedding only occurs in the vicinity of the sensor. For short times after the initiation of feedback control, vortex shedding was suppressed over most of the cylinder span, but end effects ultimately infect the entire wake except near the sensor and vortex shedding is reestablished.

Taking a cue from the limitations of the single-sensor feedback control studies, Gillies[19] developed a multiple-sensor feedback technique to achieve shedding suppression at a Reynolds number (Re=100) where earlier single-sensor approaches had failed. The rationale was that feedback control ultimately destabilizes higher order modes and single-sensor feedback cannot control all of the active modes. In this computational approach, a low-dimensional model was developed using POD to identify the global modes. A neural network was used to estimate the model coefficients from observations of the wake when subject to forcing. It was also used to design the non-linear controller. The control input was rotational oscillation of the cylinder.

Graham et al.[20] also used rotational oscillation to effect feedback control of the cylinder wake at Re = 100. They developed a low-dimensional model from Galerkin projection of the Navier-Stokes equations onto POD modes obtained from numerical simula-

tions. Optimal control theory was used in the model control. While suppression of the wake unsteadiness was achieved, the degree of suppression depended critically on the accuracy of the low-dimensional model. Moreover, the control system was found to be more complex than might be expected from inspection of the unforced wake and due primarily to the destabilization of higher order models when the wake was subjected to control.

Theoretical Development

Following the lead of Gillies[19] and Graham et al.,[20] we take the approach that the wake can be represented by a relatively low-dimensional model obtained from the Navier-Stokes equations. The Galerkin method with the proper orthogonal decomposition yields a physics-based model of the wake and permits the inclusion of higher order modes that may be destabilized during control. Below we briefly discuss how the model is developed.

Galerkin Method

A low-dimensional model for the wake is obtained from the Navier-Stokes equations using a Galerkin method, see Fletcher.[21] The global modes are obtained empirically using the proper orthogonal decomposition (POD). Velocity field measurements obtained from the experiments are used in the POD to generate the modes.

In the Galerkin approach, we do a Reynolds decomposition of the velocity field, then expand the fluctuating component in a series of time-dependent coefficients, $a_k(t)$, and spatial modes, $\phi_i^k(\mathbf{x})$.

$$u_i(\mathbf{x},t) = \sum_{k=1}^{\infty} a_k(t)\phi_i^k(\mathbf{x})$$

The individual spatial modes represent the coherent characteristic features of the fluctuating velocity field and are obtained from the POD procedure. This representation for the instantaneous velocity field is then substituted into the Navier-Stokes equations for the velocity fluctuation and projected onto the POD modes. The result is a system of first-order, nonlinear differential equations for the temporal coefficients, $a_k(t)$.

$$\frac{da_k}{dt} = F(a_k)$$

To obtain a simplified description of the flow-field, we truncate the series representation for the fluctuating velocity field at a number of modes expected to faithfully reproduce the important flow dynamics and obtain a reduced-order model of the cylinder wake. This model can then be integrated in time, using say a fourth-order Runge-Kutta scheme, to obtain the temporal coefficients.

Proper Orthogonal Decomposition

In building a low-dimensional model of the cylinder wake with a Galerkin approach, one is confronted with a decision for how to choose a characteristic set of global modes with which to expand the velocity field. In this work, we use the proper orthogonal decomposition (POD) to identify the global modes in the cylinder wake. The approach is empirical in that it uses experimentally obtained velocity realizations of the wake, but is an optimal approach in that it will capture more kinetic energy in the fewer modes than any other decomposition of the flow. A more detailed discussion of this approach can be found in Holmes et al.[22]

To summarize the POD-based approach, we are interested in obtaining a set of modes for which the average projection of the velocity field onto the modes obtains the largest value. This maximization task leads to a calculus of variations problem involving the integral equation

$$\int \mathbf{K}(\mathbf{x},\mathbf{x}')\phi(\mathbf{x}')d\mathbf{x}' = \lambda\phi(\mathbf{x})$$

where $\mathbf{K}$ is the spatial velocity correlation tensor, $\langle u_i(\mathbf{x})u_j(\mathbf{x}')\rangle$, λ are the eigenvalues and ϕ are the eigenfunctions.

In the current work, we used the Method of Snapshots developed by Sirovich.[23] This approach starts with a collection of velocity field realizations obtained experimentally

$$\mathbf{u}^n(\mathbf{x}) = \mathbf{u}(\mathbf{x}, n\tau)$$

where $\mathbf{u}$ are the velocity fluctuations and are uncorrelated for different values of n. Using the ergodic hypothesis, the spatial velocity correlation tensor may be constructed as follows

$$\mathbf{K}(\mathbf{x},\mathbf{x}') = \frac{1}{M}\sum_{n=1}^{M} \mathbf{u}^n(\mathbf{x})\left[\mathbf{u}^n(\mathbf{x}')\right]^{\mathsf{T}}$$

where $[\mathbf{u}^n(\mathbf{x}')]^{\mathsf{T}}$ is the transpose of $\mathbf{u}^n(\mathbf{x}')$ and for each $\mathbf{x}$ and $\mathbf{x}'$, $\mathbf{K}$ is the 3×3 velocity correlation matrix, given sufficiently large M.

Now $\mathbf{K}$ will have eigenfunctions of the form

$$\phi_i(\mathbf{x}) = \sum_{k=1}^{N} A_k\mathbf{u}^k(\mathbf{x})$$

Introducing $\mathbf{K}$ and ϕ_i into the integral equation, one obtains

$$\mathbf{C}_{nk}A_k = \lambda A_n$$

where

$$\mathbf{C}_{nk} = \frac{1}{M}\int [\mathbf{u}^n(\mathbf{x}')]^{\mathsf{T}}\mathbf{u}^k(\mathbf{x}')\, d\mathbf{x}' \qquad k = 1,2,3,...,M$$

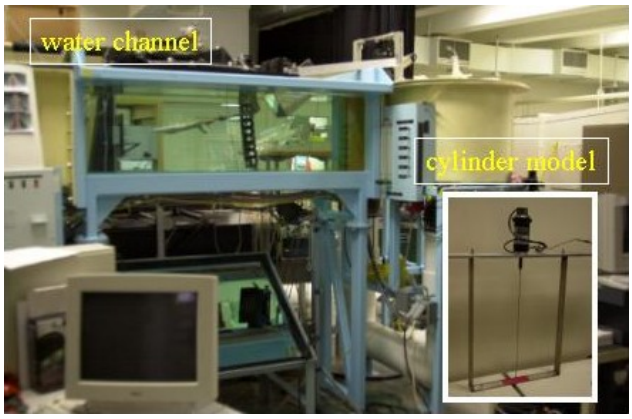

Fig. 1 Photograph of the water channel facility and circular cylinder model.

Note that each entry of $\mathbf{C}_{nk}$ is a scalar resulting from the spatial integration over all points in the pair of snapshots n, k.

The solution of the eigenvalue problem and the subsequent reconstruction procedure for $\phi_i^n(\mathbf{x})$ provides a hierarchy of characteristic spatial representations for the velocity fluctuations. This approach is particularly well-suited to PIV measurements where a finite set of velocity realizations are available rather than the velocity correlation tensor.

Experimental Measurements

The basis for the modeling of the cylinder wake is experimentally obtained velocity measurements in the wake. Here, we discuss the experimental setup, the test conditions and the data acquisition procedures. We then consider the effect of open-loop forcing on the structure of the wake by examining several representative forcing cases.

Experimental Setup

The experimental measurements were obtained in the USAFA Aeronautics Laboratory recirculating water channel. The cross section of the water channel was 38 cm by 38 cm (see figure 1), and the test section was 1.5 m in length.

The circular cylinder model was a stainless steel rod measuring 2.38 mm in diameter and 42 cm in length. To permit the cylinder to rotate about its longitudinal axis, the cylinder was mounted in two ball-bearing supports that were located on opposite sides of a rigid frame (Figure 1). The cylinder and frame were positioned vertically in the water channel, 30 cm downstream of the entrance to the test section; the frame fit flush against the channel sidewalls and bottom. A servo-motor with encoder feedback was used to effect the rotational motion.

S_f	Ω_1	daq		S_f	Ω_1	daq
0.189	0.2	A		0.248	0.2	A
0.189	0.4	A		0.248	0.4	A
0.189	0.5	A, P		0.248	0.6	A
0.189	0.6	A		0.248	1.0	A
0.189	0.65	A		0.248	1.05	A
0.189	0.7	A		0.248	1.1	A
0.189	0.75	A		0.248	1.15	A
0.189	0.8	A		0.248	1.2	A
0.189	0.85	A		0.248	1.25	A
0.189	0.9	A		0.248	1.3	A
0.189	0.95	A		0.248	1.35	A
0.189	1.0	A		0.248	1.4	A
0.189	1.2	A		0.248	1.8	A
0.189	1.4	A		0.248	2.0	A
0.189	1.5	A, P		0.248	2.4	A

Table 1 Test Conditions. A, asynchronous; P, phase-locked.

For all measurements, the freestream velocity was 6.0 cm/s. The cylinder Reynolds number based on the diameter was 125. The natural shedding frequency of the cylinder was estimated from the Strouhal number ($S_f \equiv fD/U_\infty$) at a Reynolds number of 125 and assuming parallel shedding.[24] At this Reynolds number, the Strouhal number was estimated to be 0.177 yielding a shedding frequency of approximately 4.46 hz. A spectral analysis of the temporal coefficients in the Galerkin projection revealed a shedding frequency of 4.57 hz.

In the current set of experiments, the control input was an oscillatory rotational motion about the longitudinal axis of the cylinder. The amplitude of the motion was characterized using the peak linear velocity of the cylinder surface.[11]

$$v_\theta = v_{\theta,max} \sin 2\pi f t$$

The peak velocity was non-dimensionalized by the freestream velocity yielding $\Omega_1 \equiv v_{\theta,max}/U_\infty$. In this study, we considered values of Ω_1 in the range

$$0.2 \leq \Omega_1 \leq 2.4$$

at two forcing frequencies. The forcing frequencies were 4.762 Hz, which was slightly higher than the Karman frequency due to the resolution of the motion control hardware, and 6.25 hz. These frequencies correspond to Strouhal numbers of 0.189 and 0.248, respectively. A listing of the forcing frequencies and amplitudes is shown in Table 1.

Using digital particle image velocimetry, two-dimensional velocity field measurements were obtained in the wake of the cylinder. The field of view extended from the trailing edge of the cylinder to approximately

eight cylinder diameters (8D) downstream. In all figures shown below the trailing edge of the cylinder is located at x/D = 0 and y/D = 3.8. In physical coordinates, the field of view was a 18.6 mm square. The PIV system employed a 1 Mpixel array camera. A 32×32 pixel interrogation area with 50% overlap was used in the data reduction. Each vector map was post-processed using a two-step sequence: first, a validation routine examined a 5×5 vector area and replaced rejected vectors with an averaged estimate; second, an averaging filter was applied to each 5×5 vector area to reduce noise.

The experimental data was acquired at 15 hz and asynchronously with respect to the forcing. For each case, 128 snapshots were acquired. To recreate an approximate picture of the wake during one forcing period, a reorganization of the snapshots was performed. This approach exploits the fact that the wake locks on to the forcing, and consequently it is possible to know when each snapshot was obtained during the forcing cycle relative to the first snapshot in the ensemble.

Open-loop Control Results

To provide a sense for how the rotational forcing modifies the cylinder wake, we consider a range of cases where the forcing was applied in open-loop at both forcing frequencies.

The effect of forcing amplitude near the Karman frequency is shown qualitatively in figure 2. Contours of the cross-span vorticity, ω_z, are shown for the unforced and four forcing cases ($\Omega_1 = 0.2$, 0.6, 0.9 and 1.5). The unforced and $\Omega_1 = 0.2$ cases appear very similar. With a low forcing amplitude, the forcing locks in the shedding at the forcing frequency but the character of the vortex street is largely unchanged from the unforced case. As the forcing amplitude increases, a gradual change in the wake structure is apparent. The vortices are displaced increasingly farther away from the wake centerline with increasing forcing amplitude. Ultimately, it appears that the shear layers originating from the top and bottom surfaces of the cylinder remain distinct. This structure resembles qualitatively the 'sea-horse' structure observed by Detemple-Laake and Eckelmann.[7]

Similar qualitative results were observed when forcing at $S_f = 0.248$ (see figure 3). Yet, a sequence of reordered snapshots showing lock-on in the near wake for $\Omega_1 = 1.1$ revealed that the two shear layers appear to interact near the end of the measurement domain to initiate the formation of, what appears to be, a Karman vortex street. Interestingly, this vortex street did not appear to be synchronized with the forcing. A simple conclusion drawn from these observations is that as Ω_1 increases, the formation length for the Karman street increases.

A mean velocity field can be obtained by averaging over the entire ensemble of velocity field snapshots for

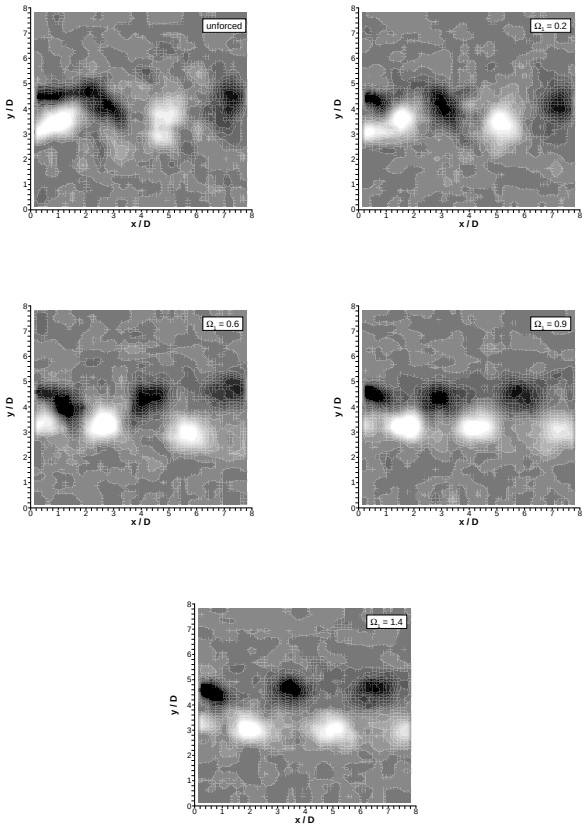

Fig. 2 Contours of the cross-span vorticity, ω_z, in the wake of the cylinder for five forcing amplitudes at $S_f = 0.189$: $\Omega_1 = 0$, 0.2, 0.6, 0.9, 1.4.

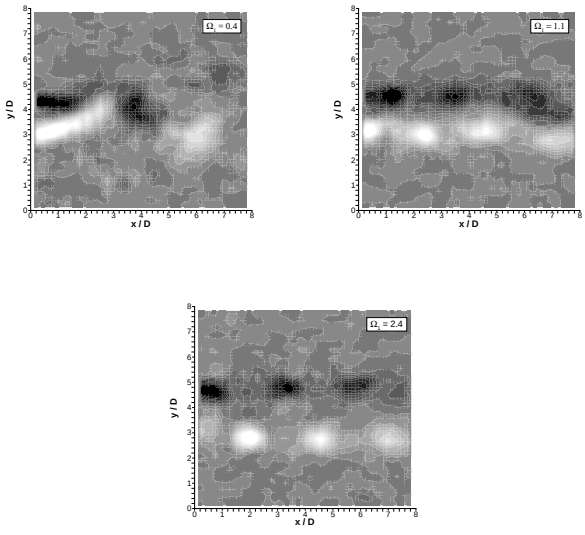

Fig. 3 Contours of the cross-span vorticity, ω_z, in the wake of the cylinder for four forcing amplitudes at $S_f = 0.248$: $\Omega_1 = 0.4$, 1.1, 2.4.

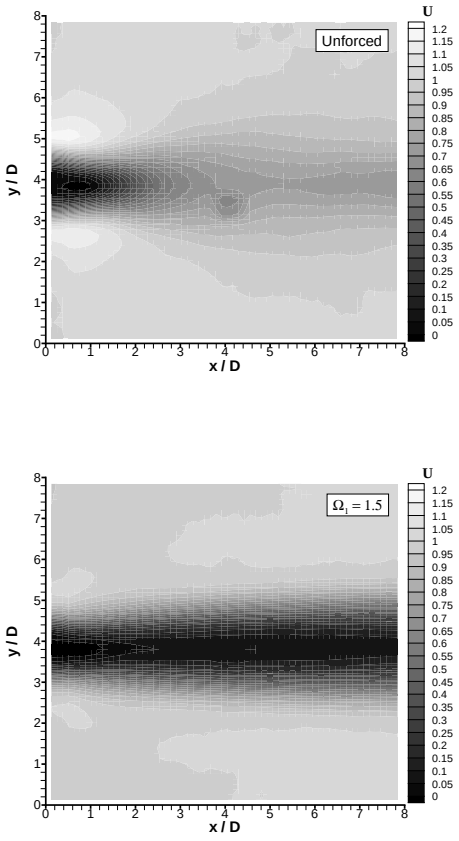

Fig. 4 Contours of the mean streamwise velocity for the unforced wake and the wake with $\Omega_1 = 1.5$ at $S_f = 0.189$.

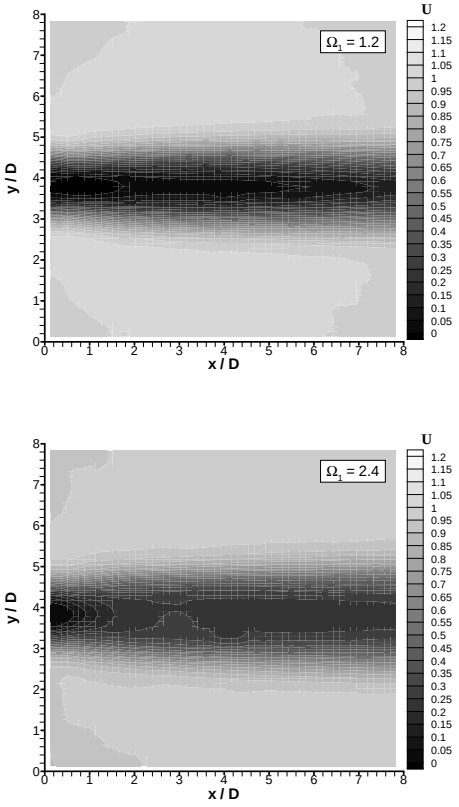

Fig. 5 Contours of the mean streamwise velocity for two forcing cases at $S_f = 0.248$, $\Omega_1 = 1.2, 2.4$

a given forcing condition. These mean velocity fields reveal a dramatic increase in the length of the mean recirculation zone as the forcing amplitude increases. Figure 4 compares contours of the mean streamwise velocity for the unforced and $\Omega_1 = 1.5$ at $S_f = 0.189$ cases. For the forced case, a region of significantly reduced velocity extends far downstream; in fact, it extends beyond the end of the measurement domain, or over eight diameters downstream of the cylinder trailing edge. Mean streamwise velocity contours at $S_f = 0.248$ reveal a similar mean wake at $\Omega_1 = 1.2$; however, at higher forcing amplitudes ($\Omega_1 = 2.4$), the low velocity region decreases in streamwise extent (figure 5). Taneda[25] shows that at yet higher forcing amplitudes ($\Omega_1 \approx 12.5$) it is possible to close the recirculation region completely.

To summarize the effects of rotational forcing on the cylinder wake at a fixed Strouhal number and with increasing forcing amplitude. We observed that the Karman vortex street appears to undergo a gradual transition from vortices of alternating sign aligned along the wake centerline to a pattern of similar vortices displaced above and below the wake centerline. This transition is observed at both forcing frequencies. Initially, as the forcing amplitude increases, the length of the mean recirculation region in the wake increases in streamwise extent. However, at the highest forcing amplitudes investigated, we observed that this region must reach at maximum at a critical value of Ω_1 and then decrease. At $S_f = 0.248$, the critical value of Ω_1 is near 1.2. At $S_f = 0.189$, the value is greater than 1.5. One can infer from this latter observation that the drag coefficient may first increase with forcing amplitude, achieve a maximum then decrease with further increases in forcing amplitude.

As mentioned above, the main focus of this work was the development of a low-dimensional model that can accurately predictive the wake dynamics with and without the rotational forcing. The following sections address this work in detail.

Wake Flow Analysis

To develop the low-dimensional model of the wake, we consider in turn the POD analysis of the wake, the Galerkin projection, from which we obtain wake models, and then the predictive quality of the models. We conclude by considering an approach for obtaining a broader set of global modes for the wake.

POD Modes

A POD analysis was performed on each data set, and the mode sets were compared to highlight the similarities and differences that appear in the wake

structure as a result of the forcing.

For each forcing case, the number of modes that may contribute significantly to the overall dynamics of the wake was evaluated by considering the eigenvalue spectra. The eigenvalues give a measure of the contribution each mode makes to the total fluctuating kinetic energy. Figure 6 shows the eigenvalues for the first 20 modes in the unforced and three forcing cases (Ω_1 = 0.2, 0.9, 1.5) at S_f = 0.189. In the unforced case, the first six modes capture 90% of the fluctuating energy. If a low level of forcing (Ω_1 = 0.2) is added to the wake, the first *two* modes capture 95% of the flow energy. That is, the low amplitude forcing locks the wake into a more coherent flow state, captured with fewer modes. Increasing the forcing amplitude to Ω_1 = 0.9 distributes the flow energy over a larger number of modes, but further increases from there appear again to lock-in a coherent flow state that is less dynamically complex.

The eigenvalues can also be used to estimate the dimensionality of the flow. For example, increasing the forcing amplitude from Ω_1 = 0.2 to 0.9, increases the number of modes that contain 90% of the kinetic energy from two to eighteen (figure 6). This observation reveals that the complexity of the flow at the higher amplitude forcing condition is quite a bit greater than at the lower forcing condition, and consequently, a higher dimensional model will be required to capture the wake dynamics accurately.

Figure 7 shows the fraction of the kinetic energy in the wake modes for cases with forcing at S_f = 0.248. Four forcing amplitudes (Ω_1 = 0.4, 1.1, 1.4, 2.4) are compared with the unforced case. A behavior similar to the S_f = 0.189 case is observed, particularly in the way that the complexity of the wake increases as the forcing amplitude increases. For example, as the amplitude of the forcing is increased from 0.4 to 1.4, the wake kinetic energy is increasingly spread over a larger number of modes. However, as the forcing amplitude continues to increase beyond 1.4, a more coherent state is locked-in, and the dimensionality of the wake is reduced. In general though, the wake appears to be more complex at this forcing Strouhal number than for forcing near the natural Strouhal number.

The eigenfunctions obtained from the POD analysis are two-dimensional vector fields. In the following discussion, we present vorticity eigenfunctions for the first four modes.

Figures 8–11 show the eigenfunctions for the unforced and three forcing cases at S_f = 0.189. For all cases, the modes appear in similar pairs with each member in a pair spatially shifted relative to the other. The unforced and Ω_1 = 0.2 case exhibit very similar mode shapes. The modes for the forced case are, perhaps, more distinct as might be expected from the eigenvalue spectra (figure 6). Recall from the raw vorticity snapshots of the wake for different forcing

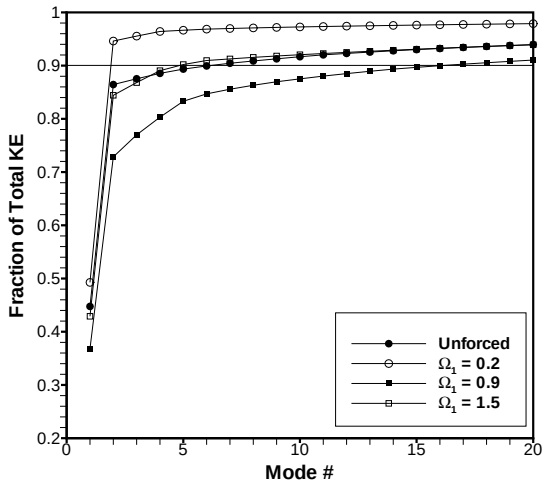

Fig. 6 A comparison of the kinetic energy contained in the first 20 modes for the cases with forcing at S_f = 0.189: Ω_1 = 0, 0.2, 0.9, 1.5.

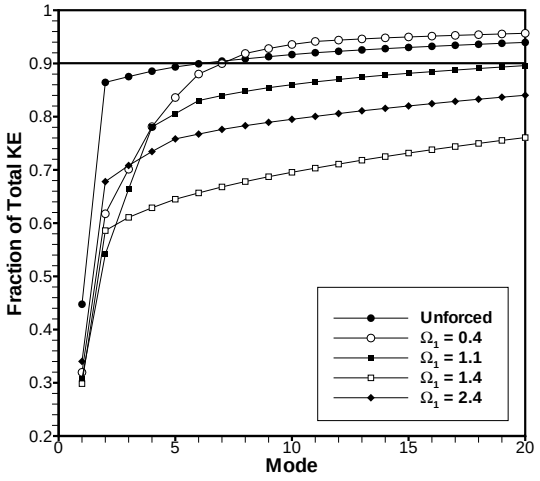

Fig. 7 A comparison of the kinetic energy contained in the first 20 modes for the cases with forcing at S_f = 0.248: Ω_1 = 0, 0.4, 1.1, 1.4, 2.4.

conditions (figure 2), the wake appears to undergo a gradual transformation as Ω_1 increases. At this value of S_f, this apparent gradual change is manifested in a relatively abrupt change in the mode shapes near Ω_1 = 0.9. Near this value of Ω_1, the two most dominant modes at the low forcing amplitude (see figure 9) disappear with two new modes appearing (see figure 10). At Ω_1 = 0.9, modes 3 and 4 are indistinct while higher modes (not shown) do appear distinct. Near this forcing amplitude boundary, mode switching takes place in the wake with the Karman vortex street becoming subordinate to a new shedding state. At Ω_1 = 1.5, the new shedding state has become energetically dominant and the new wake modes distinct.

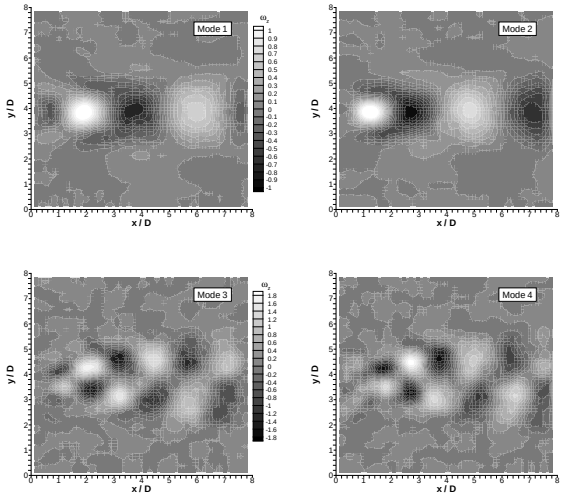

Fig. 8 Contours of the cross-span vorticity, ω_z, for the first four modes of the unforced wake.

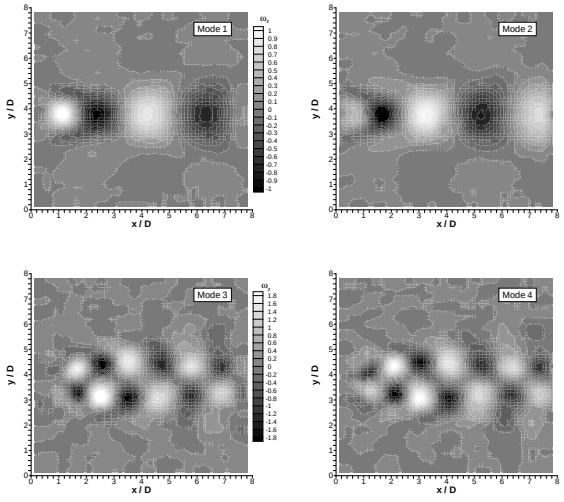

Fig. 9 Contours of the cross-span vorticity, ω_z, for the first four modes at $\Omega_1 = 0.2$ and $S_f = 0.189$.

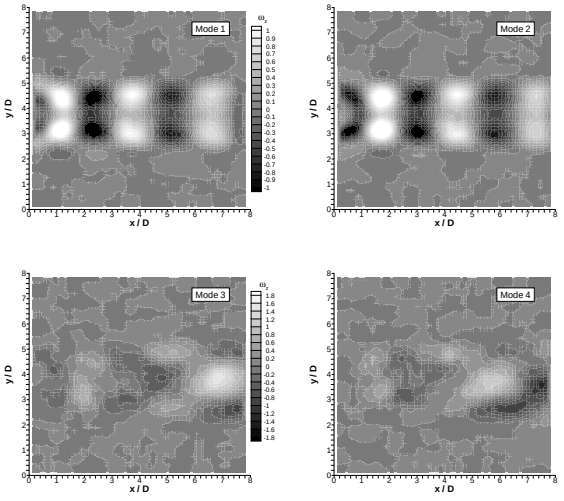

Fig. 10 Contours of the cross-span vorticity, ω_z, for the first four modes at $\Omega_1 = 0.9$ and $S_f = 0.189$.

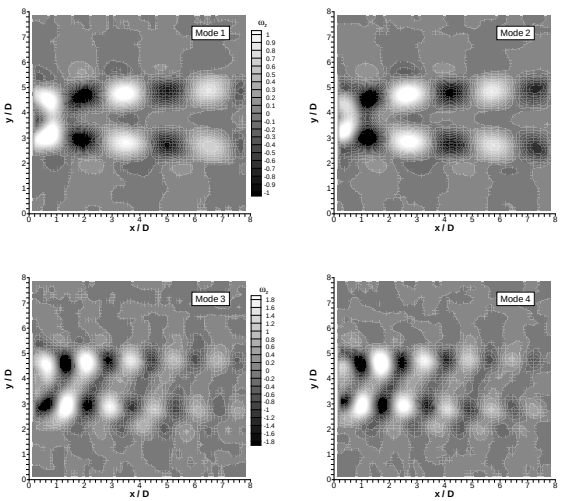

Fig. 11 Contours of the cross-span vorticity, ω_z, for the first four modes at $\Omega_1 = 1.5$ and $S_f = 0.189$.

We note that each mode pair exhibits a distinct symmetry with respect to the wake centerline. For the unforced and low amplitude forcing cases, the first two modes are symmetric with respect to the wake centerline while the next higher modes are asymmetrically arranged. At higher forcing amplitudes, a new symmetry is observed in modes 1 and 2, but the asymmetry in modes 3 and 4 appears unchanged. In addition, the wavelength of the modes has decreased by a factor of two.

The first four eigenfunctions for forcing at $S_f = 0.248$ and $\Omega_1 = 0.4$, 1.1, 2.4 are shown in figures 12–14. Qualitatively the mode shapes are similar to those found at $S_f = 0.189$. The first two modes at $\Omega_1 = 0.4$ (figure 12) are similar to the first two modes in the unforced wake (figure 8). The next two modes, however, are quite distinct from modes 3 and 4 in the unforced case, suggesting that the locked-in wake at a higher Strouhal number is structurally different to the unforced wake despite qualitative similarity in the overall wake vorticity distribution. We again observe a transition in the hierarchy of wake modes near a critical value of Ω_1. At $S_f = 0.248$, the critical value is slightly higher, 1.1, than the value at the lower Strouhal number, 0.9. Beyond $\Omega_1 = 1.1$ when the new wake state is coherently locked-in, the first four modes are essentially identical to those observed at the lower Strouhal number. However, a shorter wavelength is observed due to the higher frequency.

From inspection of the wake modes, we can infer that the wake structure is dynamically similar at two different forcing Strouhal numbers. The transition from the modes yielding the Karman vortex street to modes giving the asymmetric vortex street occurs near the non-dimensional forcing amplitude $\Omega_1 = 1.0$ at both Strouhal numbers. These observations suggest that we should be able to construct a single

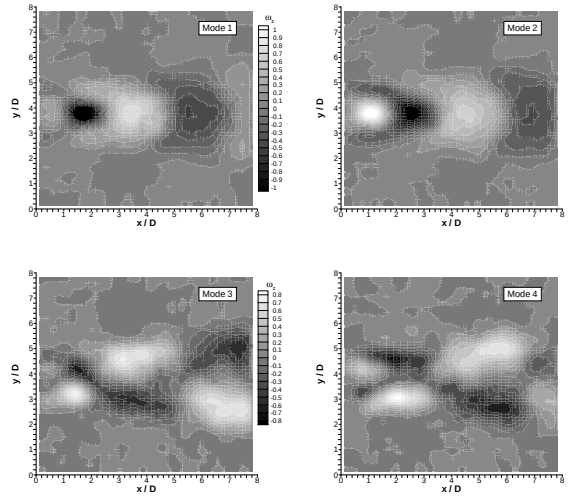

Fig. 12 Contours of the cross-span vorticity, ω_z, for the first four modes at $\Omega_1 = 0.4$ and $S_f = 0.248$.

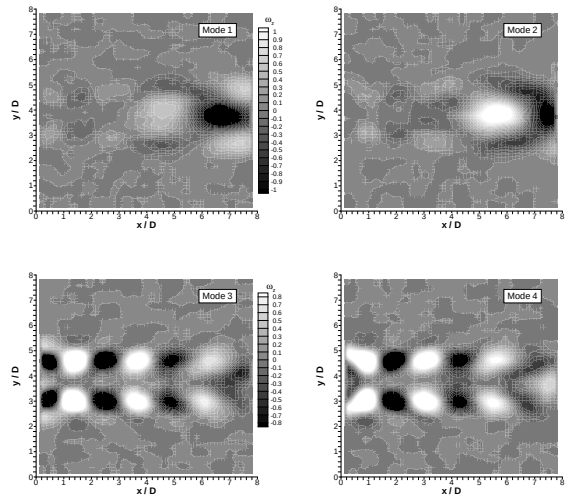

Fig. 13 Contours of the cross-span vorticity, ω_z, for the first four modes at $\Omega_1 = 1.1$ and $S_f = 0.248$.

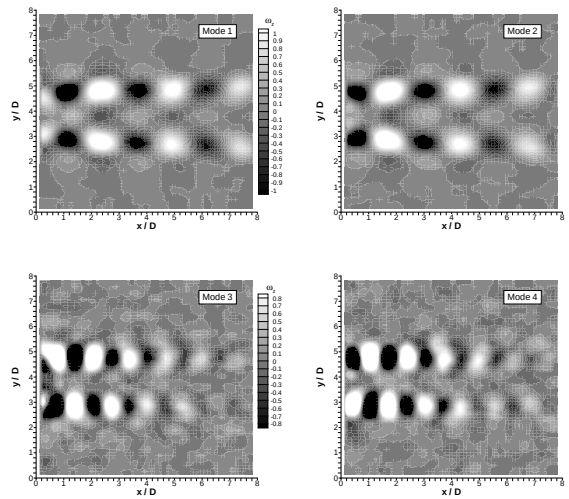

Fig. 14 Contours of the cross-span vorticity, ω_z, for the first four modes at $\Omega_1 = 2.4$ and $S_f = 0.248$.

low-dimensional model capable of capturing the wake dynamics over a range of forcing amplitudes and frequencies.

Galerkin Projection

A low-dimensional model of the wake was obtained using the Galerkin method described above. The eigenfunctions, obtained from the POD analysis, form the basis for the projection of the Navier-Stokes equations. For the open-loop control cases, a low-dimensional model was obtained for each forcing amplitude, and the predictions from the model were compared with the experimental measurements. Below we compare the predicted temporal coefficients with the temporal coefficients obtained from projections of the experimental measurements onto the POD modes at the same phase in the wake shedding cycle. Reconstructions of the temporal evolution of the wake were also made. To begin the discussion, we briefly show the general form of the low-dimensional model.

The projection of the Navier-Stokes equations onto the POD modes yields a system of first-order, nonlinear differential equations for the temporal coefficients, $a_k(t)$. The general form of this system is shown below.

$$\frac{da_k}{dt} = -(B^{kn} - \nu D^{kn})a_n - C^{knm}(a_n a_m - \delta_{nm}\overline{a_n a_m})$$

where

$$B^{kn} = \left(\phi_i^k, \langle U_j\rangle \frac{\partial \phi_i^n}{\partial x_j} + \phi_j^n \frac{\partial \langle U_i\rangle}{\partial x_j}\right)$$

$$C^{knm} = \left(\phi_i^k, \phi_j^n \frac{\partial \phi_i^m}{\partial x_j}\right)$$

$$D^{kn} = \left(\phi_i^k, \frac{\partial \phi_i^n}{\partial x_j^2}\right)$$

The parentheses ( ) indicate a suitably defined inner product, and we note that the coefficient matrices are constant for a given forcing condition.

This first-order system was truncated at a relatively low order. In this study, we considered models of order four to sixteen. No attempt was made to model the flow energy lost due to the truncation procedure. We justify this approach *a posteriori*. The truncated system was integrated using a fourth-order Runge-Kutta routine, and the solutions were found to be independent of the time step.

Figure 15 shows the temporal coefficients, a_k, predicted by the low-dimensional models for two periods of the wake oscillation. The unforced wake and the forced wake for three forcing amplitudes ($\Omega_1 = 0$, 0.2, 0.9, 1.5) at $S_f = 0.189$ are shown. A four mode model was used all cases except the $\Omega_1 = 0.9$ case where, due to the complexity of the wake, a sixteen mode model was employed. The experimental data shown in these

figures was reordered for comparison with the model predictions. To reorder the unforced data, we used an spectral analysis to estimate the shedding frequency and found it to be 4.57 hz ($S_f = 0.181$).

For the unforced wake, the noise in the projections of the experimental data makes a comparison somewhat difficult. Nevertheless, we observe that the model prediction is quite accurate in phase and amplitude. With low amplitude forcing ($\Omega_1 = 0.2$), the four mode model shows a lightly damped oscillation in the first two temporal coefficients, and the agreement with the experimental data gets worse near the end of the second oscillation. This result is somewhat surprising, as the POD analysis of the $\Omega_1 = 0.2$ case revealed a very compact wake structure with over 95% of the wake energy in the first four modes. In subsequent evaluations (not shown here), a two mode model gave slightly better agreement with little to no damping but with a slight shift in phase. The model predictions for the $\Omega_1 = 0.9$ case show the best agreement with the experimental data. This result is perhaps surprising, as this forcing amplitude is near the transition in the wake structure. Because the structure of the wake at this forcing amplitude is more complex, a higher dimensional model was required. Our initial predictions with lower dimensional models showed significant phase lag and poor agreement with amplitude. Finally, for the $\Omega_1 = 1.5$ case, we observe a phase lag in the model predictions leading to a lower predicted frequency for the wake oscillation. The predicted amplitude is damped slightly, but not as much as for the $\Omega_1 = 0.2$ case.

Figures 16–17 evaluate the reconstructions of the wake for two of the forcing cases ($\Omega_1 = 0.2,\ 0.9$) at $S_f = 0.189$. In these figures, we show four reconstructed snapshots from one forcing cycle for a qualitative evaluation; we also show a quantitative measure derived from the projection of a reconstructed image onto a raw snapshot at the same time in the forcing cycle. The order of the low-dimensional models is the same as shown in figure 15. Early in the forcing period at $\Omega_1 = 0.2$, the reconstructed wake appears qualitatively to match well with the experimental observations (figure 2). However at t/T = 0.75, the wake vortices appear to become distorted suggesting a non-physical behavior. The correlation of the reconstruction with the original wake decreases monotonically with time, but is due in large part to the shift in the relative phase of the two wakes. In this case, a two mode model gave a better comparison to the original wake, indicating that the distortion in the four mode model was due to the higher order modes. For $\Omega_1 = 0.9$, the qualitative comparison again is good with a similar monotonic decrease in the correlation. These comparisons suggest that the low-dimensional models can faithfully capture the wake dynamics for short time periods.

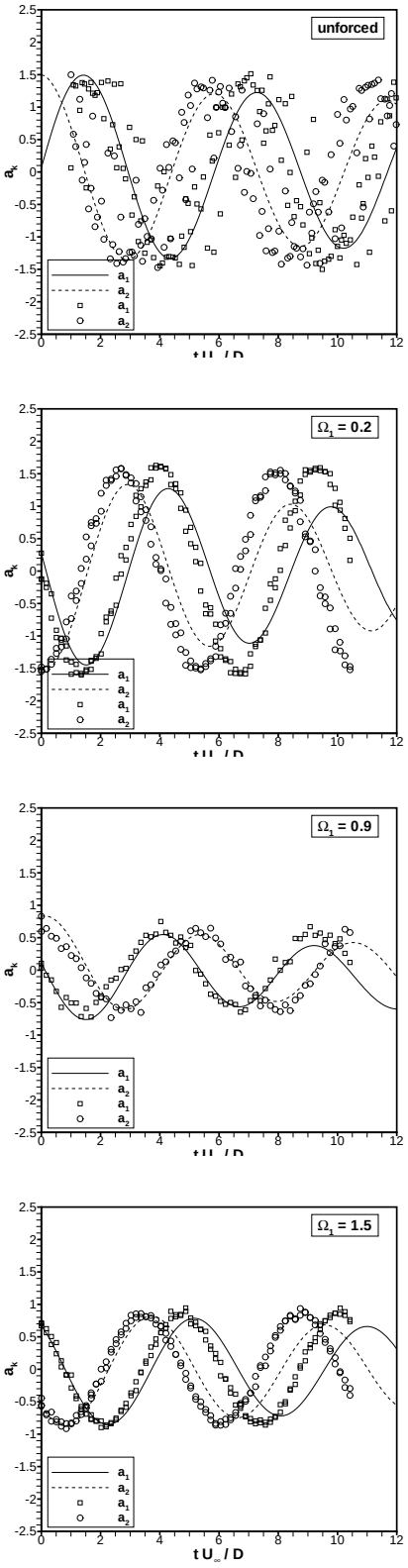

Fig. 15 Comparisons of the first two temporal coefficients from the low-dimensional models with the experimental data. Solid lines are low-dimensional model; symbols are projections of experimental data. S_f = 0.189. Ω_1 = 0.0, 0.2, 1.5, four mode models; Ω_1 =0.9, sixteen mode model.

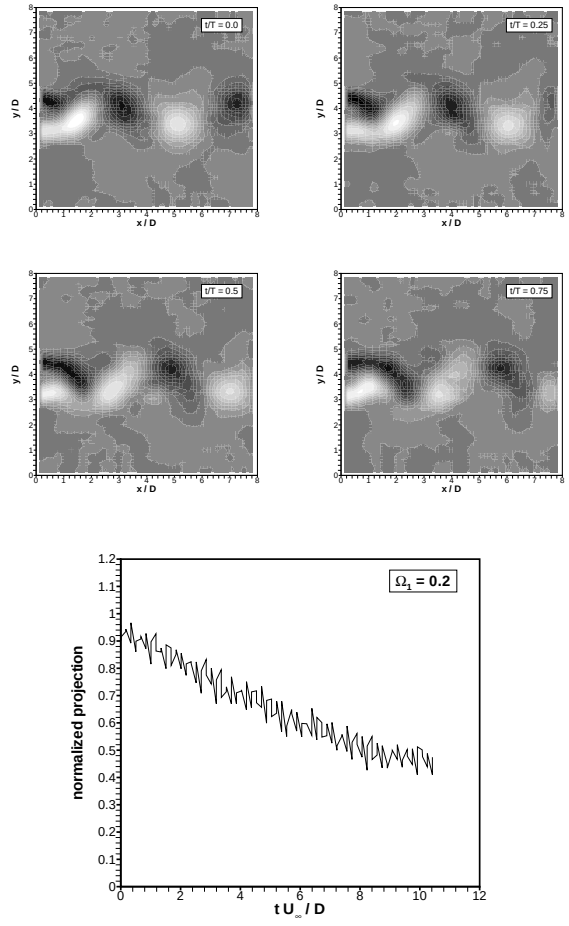

Fig. 16 The reconstructed wake from a 4 mode model for $\Omega_1 = 0.2$ and $S_f = 0.189$. Top figure shows a sequence of four reconstructed snapshots. Bottom figure shows a measure of the overall difference between the reconstructed flow and the original flow.

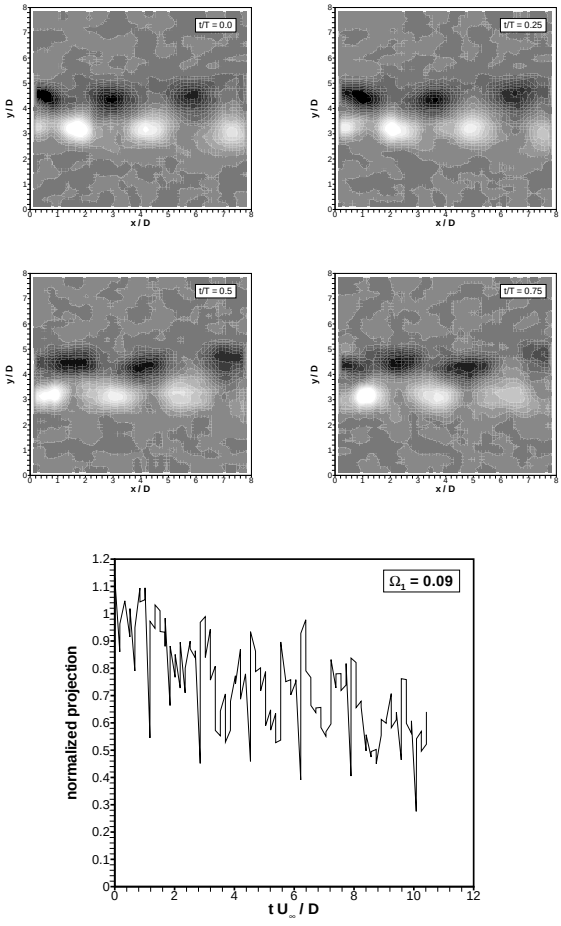

Fig. 17 The reconstructed wake from a 16 mode model for $\Omega_1 = 0.9$ and $S_f = 0.189$. Top figure shows a sequence of four reconstructed snapshots. Bottom figure shows a measure of the overall difference between the reconstructed flow and the original flow.

Data Stacking

In a flow where the control input may change the structure of the flow and create a higher dimensional system, or simply change the dominant modes, a set of modes that spans the flow through all of the control inputs is desired. This set of modes can be obtained by using an ensemble of snapshot groups where each member of the ensemble was obtained for a different value of the control input (see for example Smith and Holmes[26]).

The open-loop control cases discussed above revealed that the wake undergoes a transition from Karman shedding to an asymmetric shedding pattern near $\Omega_1 = 1.0$. At this critical value, the primary modes in the wake change, and the wake becomes more complex. After the transition, the forcing locks-in a new wake state with a different set of modes, and the dimensionality of the wake once again becomes low. To capture both types of wakes, a set of global modes must span both states.

A stacked dataset analysis was undertaken using snapshots from seven forcing amplitudes, $\Omega_1 = 0.2$, 0.4, 0.6, 0.8, 1.0, 1.2 and 1.4 at $S_f = 0.189$. The resulting general set of POD modes was then used to form a low-dimensional model for two of the forcing cases, 0.2 and 1.4. These two cases possess distinctly different wake structures and hence provide a critical test of the general applicability of the mode set. Note that the model coefficients were evaluated using the mean flow obtained from the specific forcing case. To evaluate the quality of these new models, we make three comparisons. The first comparison is with the projections of the raw velocity snapshots onto the stacked POD modes; the second comparison is with the predictions from a low-dimensional model obtained using modes from only the forced case; and the third comparison shows the correlation between the reconstructions for each case with the original snapshots. For each case shown, we have chosen the model that shows the best agreement with the experimental data, thus gaining a measure of the veracity of the models as well as the level of sophistication required to achieve it. The com-

parisons are shown in figures 18 and 19.

For $\Omega_1 = 0.2$ (figure 18), we show four mode models. The phase accuracy of the two models is comparable, but the stacked mode model appears to give a better prediction of the amplitude. Moreover, the stacked mode model retains a higher level of correlation with the original data for a longer time.

For $\Omega_1 = 1.4$ (figure 19), we compare an eighteen stacked mode model to a four mode model from the single forcing case. Both models provide good predictions for the first one and a half cycles but then appear to diverge from the experimental data. For the stacked mode model, both the phase and amplitude diverge while for the single forcing case model, only the phase appears to losing coherence. In comparing the correlations for the reconstruction and the original wake, we find that the higher dimensional model required in the stacked case to accurately predict the first couple of temporal coefficients ultimately leads to a poor correlation at later times in the reconstructed wake.

Conclusions

A set of experimental measurements in the wake of a circular cylinder undergoing low-amplitude rotational oscillations were obtained. Two forcing Strouhal numbers were considered, and the wake response to an increase in the forcing amplitude was similar at both Strouhal numbers. A transition in the wake structure was observed near $\Omega_1 = 1$: the Karman vortex street was replaced with an asymmetric, off-centerline vortex pattern. In addition, the recirculation region immediately behind the cylinder grew dramatically in the streamwise direction.

Using the experimental measurements, a low-dimensional model of the wake was obtained for each of the forcing cases considered. In each case, models of the order of four were able to qualitatively capture the vortex dynamics in the wake. In addition, a stacked dataset analysis was considered in an effort to identify a general set of wake modes for the low-dimensional model derivation. At low forcing amplitudes, the model obtained from the stacked modes worked as well as the model obtained using modes from the single forcing case. At higher forcing amplitudes, a higher dimensional model was required to obtain comparable accuracy.

For the future, we will be undertaking measurements in the cylinder wake that capture transients resulting from impulsive forcing input. We will also be working to complete the development of a low-dimensional model formulation containing a control function input. And finally, the work of Roussopoulos and Monkewitz[15] clearly shows the importance of three-dimensional effects along the span and the implications of neglecting these effects in a low-dimensional model. We will be considering the development of

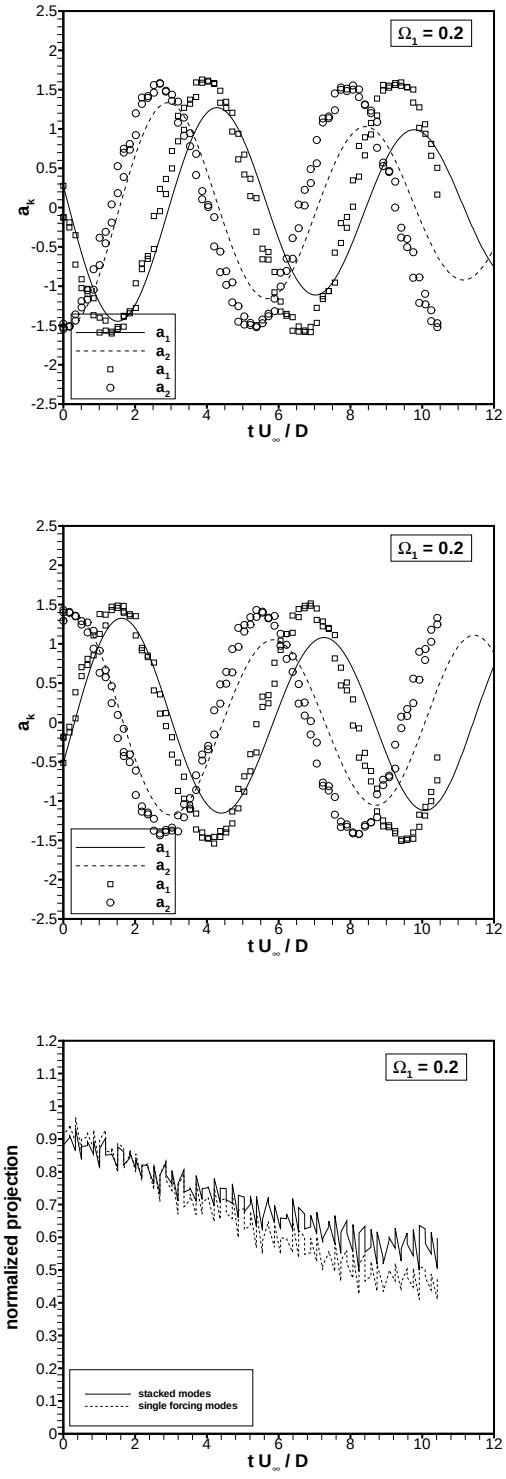

Fig. 18 Comparisons of models for the single forcing case and the stacked mode case, $\Omega_1 = 0.2$ and $S_f = 0.189$. Both models use 4 modes. First two figures show the first two temporal coefficients for the single forcing case and the stacked mode case. The bottom figure shows the correlation to the original wake for reconstructed wakes from each case.

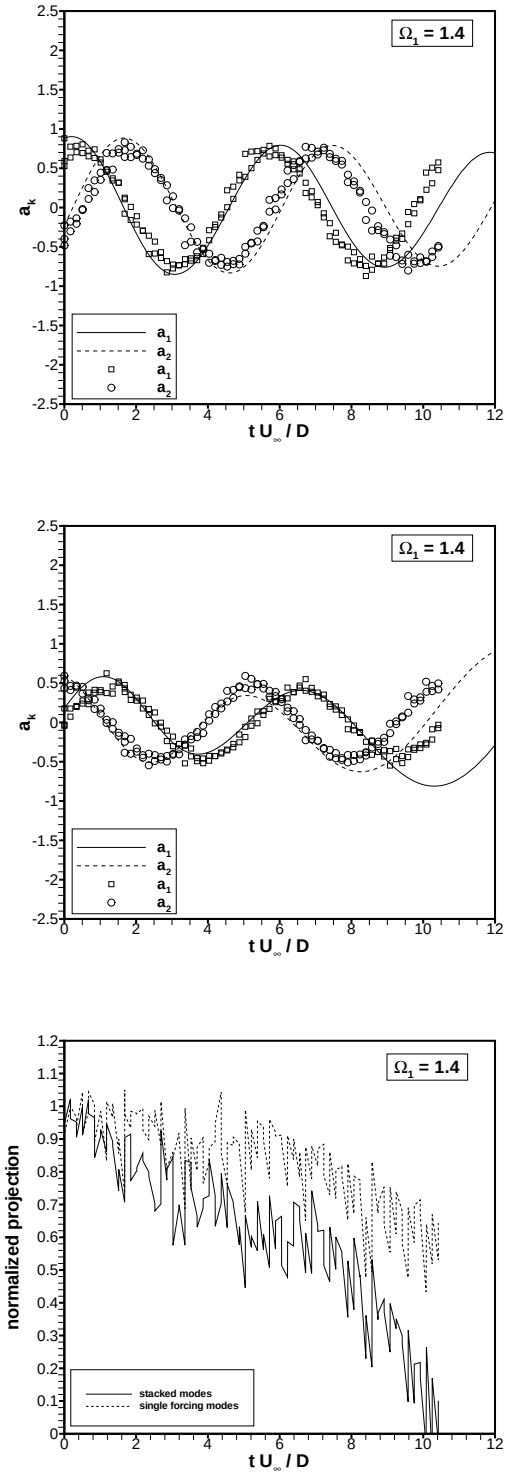

Fig. 19 Comparisons of models for the single forcing case (4 modes) and the stacked mode case (18 modes), $\Omega_1 = 1.4$ and $S_f = 0.189$. First two figures show the first two temporal coefficients for the single forcing case and the stacked mode case. The bottom figure shows the correlation to the original wake for reconstructed wakes from each case.

a hybrid low-dimensional model wherein the spanwise effects are taken into account perhaps through an adaptation from the Ginzburg-Landau equation.

Acknowledgments

The first author would like to acknowledge the support provided by the 2001 NRC/USAF Summer Faculty Fellowship program. The authors would like to acknowledge the assistance provided by Drs. Julie Morrow (USAFA) and James Myatt (AFRL/VACA).

References

[1]Abernathy, F. H. and Kronauer, R. E., "The formation of vortex sheets," *Journal of Fluid Mechanics*, Vol. 13, 1962, pp. 1–20.

[2]Koch, W., "Local instability characteristics and frequency determination of self-excited wake flows," *Journal of Sound and Vibration*, Vol. 99, No. 1, 1985, pp. 53–83.

[3]Triantafyllou, G. S., Triantafyllou, M. S., and Chryssostomidis, C., "On the formation of vortex streets behind stationary cylinders," *Journal of Fluid Mechanics*, Vol. 170, 1986, pp. 461–477.

[4]Chomaz, J. M., Huerre, P., and Redekopp, L. G., "Bifurcations to local and global modes in spatially developing flows," *Physical Review Letters*, Vol. 60, No. 1, 1988, pp. 25–28.

[5]Provansal, M., Mathis, C., and Boyer, L., "Benard-von Karman instability: transient and forced regimes," *Journal of Fluid Mechanics*, Vol. 182, 1987, pp. 1–22.

[6]Monkewitz, P., "The absolute and convective nature of instability in two-dimensional wakes at low Reynolds number," *Physics of Fluids*, Vol. 31, No. 5, 1988, pp. 999–1006.

[7]Detemple-Laake, E. and Eckelmann, H., "Phenomenology of Karman vortex streets in oscillatory flow," *Experiments in Fluids*, Vol. 7, 1989, pp. 217–227.

[8]Ffowcs Williams, J. E. and Zhao, B. C., "The active control of vortex shedding," *Journal of Fluids and Structures*, Vol. 3, 1989, pp. 115–122.

[9]Ongoren, A. and Rockwell, D., "Flow structure from an oscillating cylinder. Part 1: Mechanisms of phase shift and recovery in the near wake," *Journal of Fluid Mechanics*, Vol. 191, 1988, pp. 197–223.

[10]Wu, J., Mo, J., and Vakili, A., "On the wake of a cylinder with rotational oscillations," AIAA Paper 89-1024, 2nd AIAA Shear Flow Conference, Tempe, AZ, 13-16 March, 1989.

[11]Tokumaru, P. T. and Dimotakis, P. E., "Rotary oscillation control of a cylinder wake," *Journal of Fluid Mechanics*, Vol. 224, 1991, pp. 77–90.

[12]Filler, J. R., Marston, P. L., and Mih, W. C., "Response of the shear layers separating from a circular cylinder to small-amplitude rotational oscillations," *Journal of Fluid Mechanics*, Vol. 231, October 1991, pp. 481–499.

[13]Griffin, O. and Hall, M., "Review – vortex shedding lock-on and flow control in bluff body wakes," *Journal of Fluids Engineering - Transactions of ASME*, Vol. 113, 1991, pp. 526–537.

[14]Blevins, R. D., *Flow-Induced Vibration*, van Nostrand Reinhold, New York, 2nd ed., 1990.

[15]Roussopoulos, K. and Monkewitz, P. A., "Nonlinear modelling of vortex shedding control in cylinder wakes," *Physica D*, Vol. 97, 1996, pp. 264–273.

[16]Berger, E., "Suppression of vortex shedding and turbulence behind oscillating cylinders," *Physics of Fluids*, Vol. 10, 1967, pp. S191–s193.

[17]Roussopoulos, K., "Feedback control of vortex shedding at low Reynolds numbers," *Journal of Fluid Mechanics*, Vol. 248, 1993, pp. 267–296.

[18]Park, D. S., Ladd, D. M., and Hendricks, E. W., "Feedback control of von Karman vortex shedding behind a circular cylinder at low Reynolds numbers," *Physics of Fluids*, Vol. 6, No. 7, July 1994, pp. 2390–2405.

[19]Gillies, E., "Low-dimensional control of the circular cylinder wake," *Journal of Fluid Mechanics*, Vol. 371, 1998, pp. 157–178.

[20]Graham, W., Peraire, J., and Tang, K., "Optimal control of vortex shedding using low-order models. Part 1 – Open-loop model development," *International Journal for Numerical Methods in Engineering*, Vol. 44, 1999, pp. 945–972.

[21]Fletcher, C. A. J., *Computational Galerkin Methods*, Springer Series in Computational Physics, Springer-Verlag, 1984.

[22]Holmes, P., Lumley, J. L., and Berkooz, G., *Turbulence, Coherent Structures, Dynamical Systems and Symmetry*, Cambridge Monographs on Mechanics, Cambridge U.P., Cambridge, 1st ed., 1996.

[23]Sirovich, L., "Turbulence and the Dynamics of Coherent Structures Part 1: Coherent Structures," *Quarterly of Applied Mathematics*, Vol. 45, No. 3, 1987, pp. 561–571.

[24]Fey, U., Konig, M., and Eckelmann, H., "A new Strouhal-Reynolds number relationship for the circular cylinder in the range $47 < Re < 2 \times 10^5$," *Physics of Fluids*, Vol. 10, No. 7, July 1998, pp. 1547–1549.

[25]Taneda, S., "Visual observations of the flow past a circular cylinder performing a rotary oscillation," *Journal of the Physical Society of Japan*, Vol. 45, No. 3, 1978, pp. 1038–1043.

[26]Smith, T. and Holmes, P., "Low dimensional models with varying parameters: a model problem and flow through a diffuser with variable angle," *Fluid Mechanics and the Enviroment: Dynamical Approaches*, edited by J. L. Lumley, Springer-Verlag, 2001, pp. 315–336.